Twin-Related Grain Boundary Engineering and Its Applications

Subjects: Engineering, Mechanical

Contributor: Xiaowu Li , Xianjun Guan , Zipeng Jia , Peng Chen , Chengxue Fan , Feng Shi

The main idea of grain boundary engineering (GBE) evolves from the concept of “grain boundaries (GBs) design and control” proposed by Watanabe. In addition, after nearly 50 years of development, GBE has emerged as a mature method that can be applied to a variety of metallic materials, such as copper alloys, nickel-based alloys, austenitic stainless steels, and lead alloys.

grain boundary engineering mechanical property face-centered cubic metal

1. Introduction

Early in the 1880s, Sorby first observed with an optical microscope that the microstructure of a blister steel was composed of numerous grains of various shapes and the grain boundaries (GBs) between adjoining grains. Since then, materials researchers have paid an increasing amount of attention to the GBs and interfaces (including phase boundaries) to explore a well-established method in materials design and performance improvement [1]. After the past ~140 years of study, the understanding of GBs and interfaces has significantly improved. It is now well recognized that the GB is an important component of the microstructure in polycrystalline materials and that the number, type, and distribution of GBs play critical roles in the materials’ properties [2][3][4][5][6].

In addition, when it comes to the mechanical properties, GBs can act as the main obstacle to dislocation slip during plastic deformation, and thus become important sources of strength and work hardening of polycrystalline metallic materials [7][8]. Meanwhile, GBs may also be the preferred location for crack nucleation due to the weakened bonding strength between the atoms on both sides of the structurally disordered interface and the higher stress concentration derived from the pile-up of dislocations [9][10][11][12][13]. In addition, most noteworthy, the structural order of various GBs is significantly different [14][15][16], so that the capacity of various GBs to resist intergranular cracks is also different [10][17][18][19][20]. Therefore, cracking is most likely to occur during plastic deformation at or along ordinary random high-angle GBs (RHAGBs) with higher structural disorder and interface energy, while special GBs with low energy (will be introduced in detail later) can generally maintain a high resistance to cracking [10][11][13][21][22].

2. Twin-Related GBE

The main idea of GBE evolves from the concept of “GB design and control” proposed by Watanabe [2][3][23]. In addition, after nearly 50 years of development, GBE has emerged as a mature method that can be applied to a

variety of metallic materials, such as copper alloys [6][12][24], nickel-based alloys [25][26][27][28], austenitic stainless steels [9][10][20][29][30], and lead alloys [31][32]. These materials generally have the common characteristic that their stacking fault energies are relatively low and annealing twins (ATs) are easily formed during the thermal-mechanical process (TMP); based on this, the so-called method of twin-related GBE has been well developed.

The twin-related GBE is to induce a large number of AT boundaries (or ATs), namely Σ3 GBs, in face-centered cubic (FCC) metals by the means of thermal-mechanical treatment, and other low-Σ coincidence site lattice (CSL) GBs can be further induced through the mutual interactions between two annealing twins or even between ATs and ordinary RHAGBs, thus blocking the connectivity of RHAGBs [6][33][34][35][36]. Additionally, some previous studies [10][20][37][38] have revealed that the low-ΣCSL GBs introduced by twin-related GBE exhibit a high degree of structural stability and are not prone to second-phase precipitation during medium- to high temperature annealing or welding processes. Thus, the low-ΣCSL GBs, especially in the welding heat affected zone, often exhibit a higher corrosion resistance in corrosive environments compared with ordinary RHAGBs [39]. Moreover, many investigations [9][10][17][21][40] have substantiated that twin-related GBE is an effective way to improve the intergranular corrosion resistance, intergranular stress corrosion cracking resistance, and other properties that are closely related to GBs in some FCC metals.

Consequently, the key to the realization of GBE is to induce the formation of as many annealing twins as possible during the TMP. In addition, it should be noted that only in FCC metallic materials deformed by planar-slipping of dislocations can a large number of ATs be easily induced [6]. Therefore, the twin-related GBE can only be availably applied to some FCC metallic materials with low stacking fault energy or numerous short-range order structures [6][9][38][41][42][43]. Many important engineering materials, such as austenitic stainless steel, nickel-based alloys, and copper alloys, are involved in this kind of material, so the twin-related GBE has received widespread attention.

3. GBE-Quantifying Parameters

As mentioned above, the main purpose of twin-related GBE is to optimize the GBCD in materials, namely, increasing the fraction of low-ΣCSL GBs and blocking the connectivity of RHAGBs. In this case, it is significantly important to know how to quantify the degree of GBCD optimization. To this end, several important GBE-quantifying parameters have been successively proposed, as summarized below.

3.1. Fraction of Special GBs

The fraction of special GBs (f_{SBs}) is defined by the ratio of the length of special GBs to the total length of all GBs [20], which was most widely used in the evaluation of GBE optimization. In the statistics of f_{SBs}, the CSL GBs with $\Sigma \leq 29$ are generally regarded as the special GBs [44][45][46], since these types of GBs have lower energy [7][47][48], and exhibit some unique performances, e.g., lower diffusivity, lower resistivity, lower sensitivity to solute atom segregation, and higher resistance to GB sliding and crack initiation [7].

Furthermore, with the deepening of GBE studies, it has been recognized that, apart from the f_{SBs}, the role of special GBs is also closely related to their location, i.e., out of or in networks of random GBs. Lehockey et al. [49] reported that the coherent Σ3 GBs were dominant in all special GBs in FCC metals with low stacking fault energy; however, most of these coherent Σ3 GBs were localized outside of RHAGB networks and cannot make any positive contributions to the tailoring of RHAGB networks. Naturally, it is difficult for these coherent Σ3 GBs to impede the intergranular stress corrosion along RHAGBs. Therefore, Lehockey et al. [49] proposed the concept of effective special GBs and suggested that only the special GBs that can block the network connectivity of the random high-angle GBs are effective in preventing the failure of materials along GBs. However, the difference in the anti-cracking properties of the same type of special GBs was even sometimes reported [20][50], so that there was as yet no unified opinion on the definition of effective special GBs. Further, it may be related to the fact that the interface index is still not considered in the current electron backscatter diffraction (EBSD) characterization. Thus, the further developments in the theory of GBs and the relevant characterization methods need to be emphasized for the better application of GBE.

3.2. Distribution of Triple-Junctions

The ultimate purpose of twin-related GBE treatment is to interrupt the network connectivity of RHAGBs and thus hinder crack propagation along RHAGBs. Therefore, how to quantify the blocking of RHAGB by the GBCD optimization is of great significance for GBE. Kumar et al. [51] proposed that the connectivity of RHAGBs can be evaluated by the statistics on the distribution of triple-junctions, which are classified as different types according to the number of special GBs they contain. For example, triple-junctions with zero, one, two, and three low-energy special CSL GBs are classified as J0, J1, J2, and J3 junctions, respectively. Among these triple-junctions, the RHAGBs are interconnected with each other at the J0 and J1 junctions, and thereby cracks can pass through the junctions without hindrance and propagate along the RHAGBs. In contrast, J3 junctions are generally too stable to meet the conditions for crack nucleation and propagation. Only at the J2 junctions can the cracks be captured by special GBs. Hence, the capture probability of cracks can be quantified by statistically calculating the distribution of $f_{J2}/(1 - f_{J3})$, where f_{J2} and f_{J3} represent the proportion of J2 and J3 junctions, respectively. Several experimental studies [6][20][52] have confirmed that there indeed exists a strongly positive correlation between the $f_{J2}/(1 - f_{J3})$ and the blocking degree of RHAGB connectivity in FCC metals.

3.3. Ratio of Twin Related Domain Size to Grain Size

In the study on the mechanism of twin-related GBE, it has recently been realized that the formation of annealing twins during TMP plays an important role in increasing the f_{SBs} and interrupting the network connectivity of RHAGBs, since efficiently inducing the formation of ATs can not only directly increase the fraction of special GBs but also be beneficial to decreasing the grain size. Furthermore, the quasi-in situ EBSD observation on the evolution of GBCD further indicated that the formation and growth of ATs indeed played a critical role in GBCD optimization [33]. For example, the f_{SBs} in a GBE- treated material are directly related to the number of ATs in a twin-related domain (TRD), which is defined as $\Sigma 3^n$ twin cluster (namely, a large cluster of spatially adjacent twin-related

grains). In light of this, Barr et al. [33] suggested that the ratio *v* of TRD size to grain size should be another important indicative indicator of GBE in polycrystalline materials.

4. Mechanism of GBCD Optimization—"Twin Cluster Growth" Model

At the turn of the century, the study on the mechanism of GBCD optimization in FCC metallic materials has drawn immense attention from researchers, and several theoretical models for GBE have been proposed in succession, as shown in **Figure 1**. As a result, the "Σ3 GB regeneration model" [53] indicates that the coherent AT boundaries in different recrystallized grains can interact with each other to induce the formation of Σ9 GBs, and then the mobile Σ9 GBs further interact with some other Σ3 GBs, thus inducing the formation of other low-energy SBs (**Figure 1**a). The "high ΣCSL GB decomposition model" [54] suggests that the low-ΣCSL SBs can be derived from the decomposition of high-ΣCSL GBs (**Figure 1**b). According to the "special fragment model" [17], the GBCD optimization is mainly realized by the SB fragments caused by AT emitting in the RHAGB network (**Figure 1**c). The "incoherent Σ3 GB migration model" [55] indicates that the formation of SBs is mainly achieved by the migration of incoherent Σ3 GBs (**Figure 1**d). However, even though these models can explain some laws of GBCD evolution in FCC metals with low stacking fault energy to a certain extent, there still exist some obvious inadequacies due to the lack of understanding of the microstructure evolution during the TMP. On the basis of summarizing the recent in situ or quasi-in situ observations on the microstructure evolution of FCC metals, the "twin cluster growth" model is further introduced below.

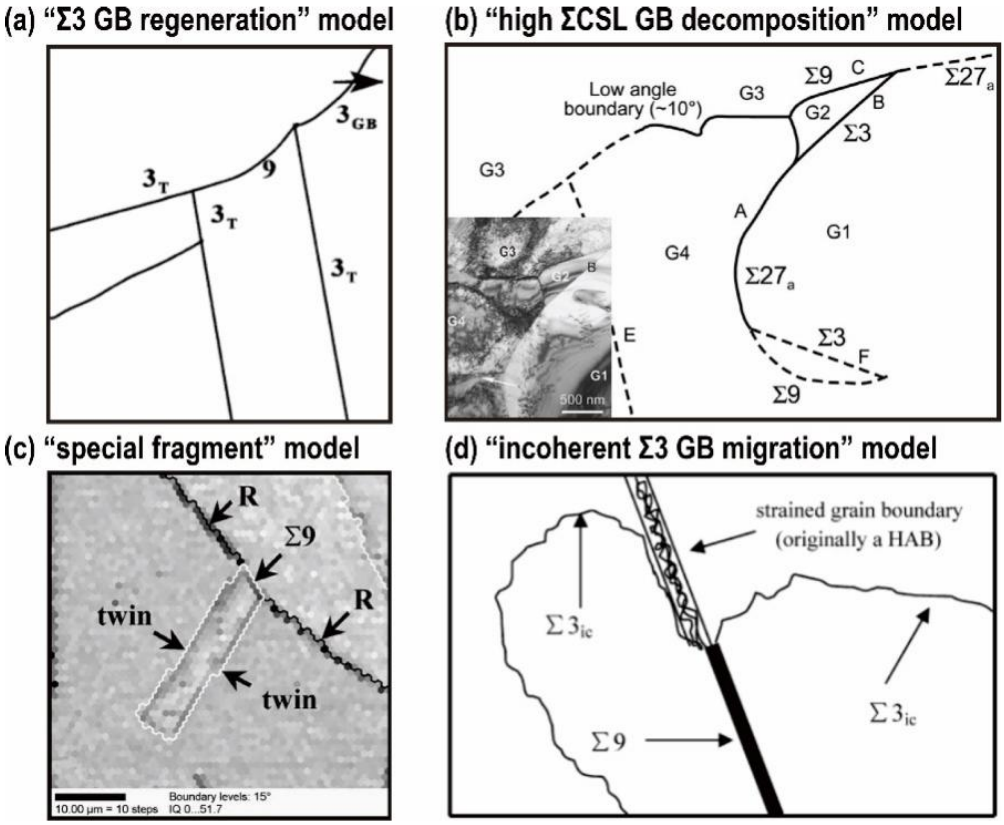

Figure 1. Theoretical models for the GBCD optimization in FCC metals Adopted from Refs. [17][53][54][55].

Additionally, through the quasi-in situ or in situ observation of the GBCD evolution during the TMP of some FCC metals (e.g., 304, 316L austenitic stainless steels, and copper alloys) [6][33][56], it has been well recognized that the microstructural evolution during GBE treatment is mainly completed by strain-induced GB migration. For example, the ordinary RHAGBs driven by the stored strain energy migrate from the twin clusters to the deformed matrix during the annealing process of the TMP, and ATs are constantly nucleated behind the migrating GBs and grow up with the migration of GBs, as shown in **Figure 2**. Therefore, inducing the nucleation of as many ATs as possible is crucial to realizing the optimization of GBCD in the process. First, the nucleation of ATs, as mentioned above, can directly increase the f_{SBs}. Second, ATs with different orientations nucleated behind RHAGBs may interact with each other, thus inducing other low-energy CSL special GBs (see **Figure 2**b,c). Finally, the formation of ATs can induce the structural transition of migrating RHAGBs from disorder to order, which are implanted in the network of RHAGBs and thus interrupt the network connectivity.

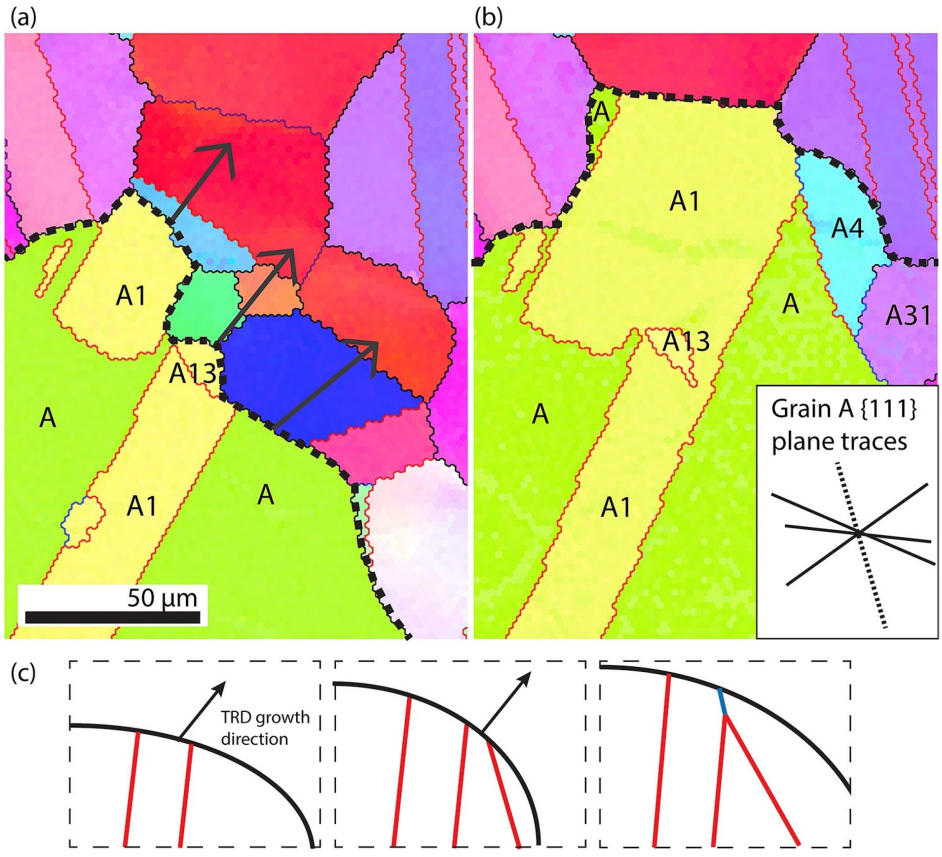

Figure 2. (**a**,**b**) Evolution of the twin cluster during the annealing process, where the dashed line indicates the interface between the existing twin cluster and the deformed matrix; (**c**) schematic of the formation of the AT boundary during the evolution of the twin cluster front and the formation of Σ9 GB (the inset illustrates the 111 plane trace for the growing grain (A). adopted from Ref. [33].

Recent studies [6][52] have shown that the deformation microstructures, including stacking faults, planar-slip dislocation structures, and deformation twins, exhibit distinctive effects on the evolution of twin clusters and thus on

the GBCD optimization, as evidenced by the experimental findings of Cu-16at.% Al alloys in **Figure 3**. The stacking faults and planar-slip dislocation structures are fairly beneficial to the GBCD optimization, for which the formation of ATs can be induced by the ordered defects in a sequence of closely packed atomic planes at the front end of a growing twin cluster. On the contrary, deformation twins hinder the growth of twin clusters, thus impairing GBCD optimization. Therefore, the optimal prior strain for the GBCD optimization should be around the threshold strain for the appearance of deformation twins in FCC metals.

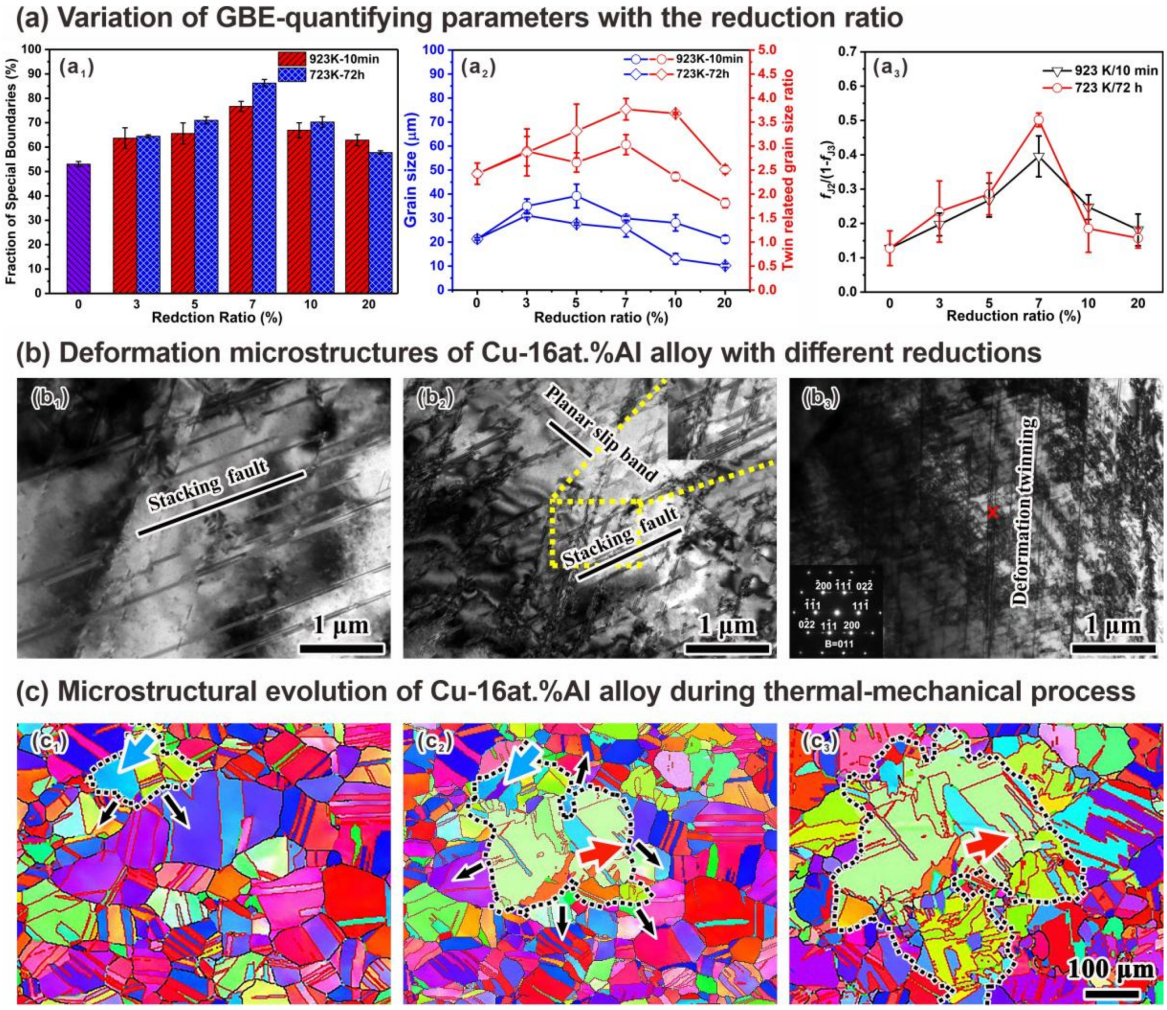

Figure 3. Influence of deformation microstructures on the GBCD optimization of the Cu-16at.%Al alloy (**a**) Variation of GBE-quantifying parameters (a_1: f_{SBs}, a_2: ratio of twin- related domain size to grain size, a_3: triple-junction distribution) with the reduction ratio; (**b**) deformation microstructures at low (3%, b_1), optimal (7%, b_2), and high (20%, b_3) reductions; (**c**) quasi-in situ EBSD observations on the evolution of microstructures during TMP treatment at an optimal stain (7% reduction, c_1) and annealing at 723 K for 12 h (c_2) and 36 h (c_3). Adopted from Ref. [6].

In addition, some low ΣCSL GBs can also be formed when two separate twin cluster migration fronts meet together during the TMP [33][56]. These special GBs must be located in the network of random high-angle GBs, which can effectively block the connectivity of RHAGB networks.

Figure 4 shows the schematic diagram of the “twin cluster growth” model obtained by summing up the above research results. In the model, the ATs in twin clusters are mainly induced by the planar deformation microstructures, including stacking faults and planar dislocation structures, which are the main source of special GBs. For example, once the stacking faults in deformation microstructures encounter migrating RHAGBs, can they strongly affect a sequence of close-packed planes of recrystallizing grain and induce the transformation from a regular sequence (… ABC …) to an inverse sequence (… CBA …), as displayed in **Figure 4**. This is because there is a a6[112¯] displacement between atoms in stacking faults and in perfect crystal. The displacement can effectively reduce the necessary energy of twinning, i.e., the stacking faults can provide excessive activation energy for twinning [33][56]. Furthermore, in a twin cluster, ATs with different orientations interact with each other as they grow with the migration of RHAGBs, thus inducing some other special GBs. Further, at the final stage of twin cluster evolution, the intersection between separate twin clusters also induces certain special GBs. Finally, the GBCD optimization of FCC metals is fully realized by the growth of twin clusters.

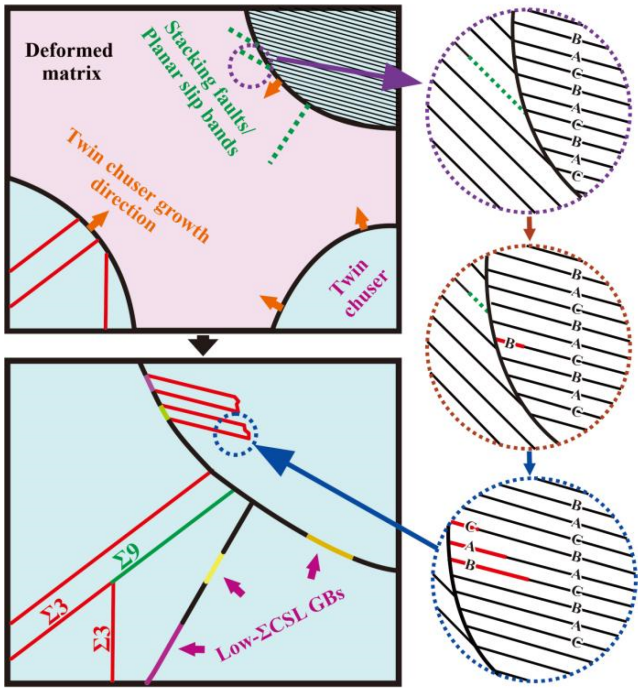

Figure 4. Schematic diagram of the “twin cluster growth” model for the GBCD optimization in FCC metals.

During the growth of twin clusters, some non-symemtric low ΣCSL GBs can also migrate in one twin cluster, such as incoherent Σ3 GBs, can reduce the interfacial energy by interacting with other special GBs in the cluster [57][58][59]. However, such behavior is not necessarily conducive to the increase of f_{SBs} (e.g., the disappearance of the AT boundary in **Figure 2**).

References

1. Hondros, E.D. Reproduced optical micrograph from Sorby HC (1887). In The Donald McLean Symposium on Structural Materials: Engineering Application through Scientific Insight; Institute of Materials Cambridge University Press: Cambridge, UK, 1996; p. 1.
2. Watanabe, T. An approach to grain boundary design for strong and ductile polycrystals. Res. Mech. 1984, 11, 47–84.
3. Aust, K.T. Grain Boundary Engineering. Can. Metall. Quart. 1994, 33, 265–274.
4. Watanabe, T. Grain boundary engineering: Historical perspective and future prospects. J. Mater. Sci. 2011, 46, 4095–4115.
5. Randle, V. Grain boundary engineering: An overview after 25 years. Mater. Sci. Technol. 2013, 26, 253–261.
6. Guan, X.; Shi, F.; Ji, H.; Li, X. Gain boundary character distribution optimization of Cu-16at.%Al alloy by thermomechanical process: Critical role of deformation microstructure. Mater. Sci. Eng. A 2019, 765, 138299.
7. Meyers, M.A.; Chawla, K.K. Mechanical Behavior of Materials; Cambridge University Press: Cambridge, UK, 2009.
8. Hosford, W.F. Mechanical Behavior of Materials; Cambridge University Press: New York, NY, USA, 2005.
9. Qi, J.; Huang, B.; Wang, Z.; Ding, H.; Xi, J.; Fu, W. Dependence of corrosion resistance on grain boundary characteristics in a high nitrogen CrMn austenitic stainless steel. J. Mater. Sci. Technol. 2017, 33, 1621–1628.
10. Shi, F.; Gao, R.-H.; Guan, X.-J.; Liu, C.-M.; Li, X.-W. Application of Grain Boundary Engineering to Improve Intergranular Corrosion Resistance in a Fe–Cr–Mn–Mo–N High-Nitrogen and Nickel-Free Austenitic Stainless Steel. Acta Met. Sin. 2020, 33, 789–798.
11. Dong, X.; Li, N.; Zhou, Y.; Peng, H.; Qu, Y.; Sun, Q.; Shi, H.; Li, R.; Xu, S.; Yan, J. Grain boundary character and stress corrosion cracking behavior of Co-Cr alloy fabricated by selective laser melting. J. Mater. Sci. Technol. 2021, 93, 244–253.
12. Guan, X.; Shi, F.; Ji, H.; Li, X. A possibility to synchronously improve the high-temperature strength and ductility in face-centered cubic metals through grain boundary engineering. Scr. Mater. 2020, 187, 216–220.
13. Guan, X.; Jia, Z.; Liang, S.; Shi, F.; Li, X. A pathway to improve low-cycle fatigue life of face-centered cubic metals via grain boundary engineering. J. Mater. Sci. Technol. 2022, 113, 82–89.
14. Shibata, N.; Oba, F.; Yamamoto, T.; Ikuhara, Y. Structure, energy and solute segregation behaviour of symmetric tilt grain boundaries in yttria-stabilized cubic zirconia. Philos. Mag. 2004, 84, 2381–2415.

15. Brandon, D. The structure of high-angle grain boundaries. Acta Met. 1966, 14, 1479–1484.
16. Sutton, A.P.; Balluffi, R.W. Interfaces in Crystalline Materials; Clarendon: Oxford, UK, 1995.
17. Shimada, M.; Kokawa, H.; Wang, Z.; Sato, Y.; Karibe, I. Optimization of grain boundary character distribution for intergranular corrosion resistant 304 stainless steel by twin-induced grain boundary engineering. Acta Mater. 2002, 50, 2331–2341.
18. Balluffi, R. Grain Boundary Structure and Properties. Master's Thesis, Massachusetts Institute of Technology, Cambridge, MA, USA, 1979.
19. Laws, M.; Goodhew, P. Grain boundary structure and chromium segregation in a 316 stainless steel. Acta Met. Mater. 1991, 39, 1525–1533.
20. Shi, F.; Tian, P.; Jia, N.; Ye, Z.; Qi, Y.; Liu, C.; Li, X. Improving intergranular corrosion resistance in a nickel-free and manganese-bearing high-nitrogen austenitic stainless steel through grain boundary character distribution optimization. Corros. Sci. 2016, 107, 49–59.
21. Michiuchi, M.; Kokawa, H.; Wang, Z.; Sato, Y.; Sakai, K. Twin-induced grain boundary engineering for 316 austenitic stainless steel. Acta Mater. 2006, 54, 5179–5184.
22. Pradhan, S.; Bhuyan, P.; Mandal, S. Individual and synergistic influences of microstructural features on intergranular corrosion behavior in extra-low carbon type 304L austenitic stainless steel. Corros. Sci. 2018, 139, 319–332.
23. Randle, V.; Ralph, B. Applications of Grain Boundary Engineering to Anomalous Grain Growth. MRS Proc. 1988, 122, 419–424.
24. King, W.E.; Schwartz, A.J. Toward Optimization of the Grain Boundary Character Distribution in OFE Copper. Scr. Mater. 1998, 38, 449–455.
25. Tan, L.; Ren, X.; Sridharan, K.; Allen, T. Corrosion behavior of Ni-base alloys for advanced high temperature water-cooled nuclear plants. Corros. Sci. 2008, 50, 3056–3062.
26. Tan, L.; Sridharan, K.; Allen, T.; Nanstad, R.; McClintock, D. Microstructure tailoring for property improvements by grain boundary engineering. J. Nucl. Mater. 2008, 374, 270–280.
27. Cao, W.; Xia, S.; Bai, Q.; Zhang, W.; Zhou, B.; Li, Z.; Jiang, L. Effects of initial microstructure on the grain boundary network during grain boundary engineering in Hastelloy N alloy. J. Alloys Compd. 2017, 704, 724–733.
28. Li, H.; Mao, Q.; Zhang, M.; Zhi, Y. Effects of aging temperature and grain boundary character on carbide precipitation in a highly twinned nickel-based superalloy. Philos. Mag. 2021, 101, 1274–1288.
29. Gao, J.; Tan, J.; Wu, X.; Xia, S. Effect of grain boundary engineering on corrosion fatigue behavior of 316LN stainless steel in borated and lithiated high-temperature water. Corros. Sci. 2019, 152,

190–201.

30. Segura, I.; Murr, L.; Terrazas, C.; Bermudez, D.; Mireles, J.; Injeti, V.; Li, K.; Yu, B.; Misra, R.; Wicker, R. Grain boundary and microstructure engineering of Inconel 690 cladding on stainless-steel 316L using electron-beam powder bed fusion additive manufacturing. J. Mater. Sci. Technol. 2019, 35, 351–367.
31. Wang, W.; Yin, F.; Guo, H.; Li, H.; Zhou, B. Effects of recovery treatment after large strain on the grain boundary character distributions of subsequently cold rolled and annealed Pb–Ca–Sn–Al alloy. Mater. Sci. Eng. A 2008, 491, 199–206.
32. Wang, W.; Zhou, B.; Rohrer, G.S.; Guo, H.; Cai, Z. Textures and grain boundary character distributions in a cold rolled and annealed Pb–Ca based alloy. Mater. Sci. Eng. A 2010, 527, 3695–3706.
33. Barr, C.M.; Leff, A.C.; Demott, R.W.; Doherty, R.D.; Taheri, M.L. Unraveling the origin of twin related domains and grain boundary evolution during grain boundary engineering. Acta Mater. 2018, 144, 281–291.
34. Sharma, N.K.; Shekhar, S. New perspectives on twinning events during strain-induced grain boundary migration (SIBM) in iteratively processed 316L stainless steel. J. Mater. Sci. 2021, 56, 792–814.
35. Jin, Y.; Lin, B.; Bernacki, M.; Rohrer, G.; Rollett, A.; Bozzolo, N. Annealing twin development during recrystallization and grain growth in pure nickel. Mater. Sci. Eng. A 2014, 597, 295–303.
36. Schuh, C.A.; Kumar, M.; King, W.E. Analysis of grain boundary networks and their evolution during grain boundary engineering. Acta Mater. 2003, 51, 687–700.
37. Hu, H.; Zhao, M.; Rong, L. Retarding the precipitation of η phase in Fe-Ni based alloy through grain boundary engineering. J. Mater. Sci. Technol. 2020, 47, 152–161.
38. Devaraj, A.; Kovarik, L.; Kautz, E.; Arey, B.; Jana, S.; Lavender, C.; Joshi, V. Grain boundary engineering to control the discontinuous precipitation in multicomponent U10Mo alloy. Acta Mater. 2018, 151, 181–190.
39. Kokawa, H. Weld decay-resistant austenitic stainless steel by grain boundary engineering. J. Mater. Sci. 2005, 40, 927–932.
40. Shi, F.; Yan, L.; Hu, J.; Wang, L.F.; Li, T.Z.; Li, W.; Guan, X.J.; Liu, C.M.; Li, X.W. Improving Intergranular Stress Corrosion Cracking Resistance in a Fe–18Cr–17Mn–2Mo–0.85N Austenitic Stainless Steel through Grain Boundary Character Distribution Optimization. Acta Met. Sin. 2022, 35, 1849–1861.
41. Han, D.; Zhang, Y.; Li, X. A crucial impact of short-range ordering on the cyclic deformation and damage behavior of face-centered cubic alloys: A case study on Cu-Mn alloys. Acta Mater. 2021,

205, 116559.

42. Irukuvarghula, S.; Hassanin, H.; Cayron, C.; Attallah, M.; Stewart, D.; Preuss, M. Evolution of grain boundary network topology in 316L austenitic stainless steel during powder hot isostatic pressing. Acta Mater. 2017, 133, 269–281.
43. Kwon, Y.J.; Jung, S.P.; Lee, B.J.; Lee, C.S. Grain boundary engineering approach to improve hydrogen embrittlement resistance in FeMnC TWIP steel. Int. J. Hydrogen Energ. 2018, 43, 10129–10140.
44. Lin, P.; Palumbo, G.; Erb, U.; Aust, K. Influence of grain boundary character distribution on sensitization and intergranular corrosion of alloy 600. Scr. Met. Mater. 1995, 33, 1387–1392.
45. Palumbo, G.; Aust, K. Structure-dependence of intergranular corrosion in high purity nickel. Acta Met. Mater. 1990, 38, 2343–2352.
46. Lehockey, E.M.; Brennenstuhl, A.M.; Palumbo, G.; Lin, P. Electrochemical noise for evaluating susceptibility of lead-acid battery electrodes to intergranular corrosion. Br. Corros. J. 1998, 33, 29–36.
47. Randle, V. The Role of the Coincidence Site Lattice in Grain Boundary Engineering; Institute of Materials: London, UK, 1996.
48. Priester, L. Grain Boundaries: From Theory to Engineering; Springer Series in Materials Science; Springer Science & Business Media: Dordrecht, The Netherlands, 2013.
49. Lehockey, E.; Brennenstuhl, A.; Thompson, I. On the relationship between grain boundary connectivity, coincident site lattice boundaries, and intergranular stress corrosion cracking. Corros. Sci. 2004, 46, 2383–2404.
50. Jones, R.; Randle, V. Sensitisation behaviour of grain boundary engineered austenitic stainless steel. Mater. Sci. Eng. A 2010, 527, 4275–4280.
51. Kumar, M.; King, W.E.; Schwartz, A.J. Modifications to the microstructural topology in f.c.c. materials through thermomechanical processing. Acta Mater. 2000, 48, 2081–2091.
52. Guan, X.; Shi, F.; Jia, Z.; Li, X. Grain boundary engineering of AL6XN super-austenitic stainless steel: Distinctive effects of planar-slip dislocations and deformation twins. Mater. Charact. 2020, 170, 110689.
53. Randle, V. Mechanism of twinning-induced grain boundary engineering in low stacking-fault energy materials. Acta Mater. 1999, 47, 4187–4196.
54. Kumar, M.; Schwartz, A.J.; King, W.E. Microstructural evolution during grain boundary engineering of low to medium stacking fault energy fcc materials. Acta Mater. 2002, 50, 2599–2612.

55. Wang, W.; Guo, H. Effects of thermo-mechanical iterations on the grain boundary character distribution of Pb-Ca-Sn-Al alloy. Mater. Sci. Eng. A 2007, 445–446, 155–162.
56. Tokita, S.; Kokawa, H.; Sato, Y.S.; Fujii, H.T. In situ EBSD observation of grain boundary character distribution evolution during thermomechanical process used for grain boundary engineering of 304 austenitic stainless steel. Mater. Charact. 2017, 131, 31–38.
57. Straumal, B.B.; Kogtenkova, O.A.; Gornakova, A.S.; Sursaeva, V.G.; Baretzky, B. Review: Grain boundary faceting–roughening phenomena. J. Mater. Sci. 2016, 51, 382–404.
58. Sursaeva, V.G.; Straumal, B.B.; Gornakova, A.S.; Shvindlerman, L.S.; Gottstein, G. Effect of faceting on grain boundary motion in Zn. Acta Mater. 2008, 56, 2728–2734.
59. Straumal, B.B.; Polyakov, S.A.; Mittemeijer, E.J. Temperature influence on the faceting of Σ3 and Σ9 grain boundaries in Cu. Acta Mater. 2006, 54, 167–172.